NANO LETTERS

2007
Vol. 7, No. 12
3864−3868

Plasma within Templates: Molding Flexible Nanocrystal Solids into Multifunctional Architectures

Arya Ghadimi, Ludovico Cademartiri, Ulrich Kamp, and Geoffrey A. Ozin*

Materials Chemistry and Nanochemistry Research Group, Center for Inorganic and Polymeric Nanomaterials, Chemistry Department, University of Toronto, 80 St. George Street, Toronto, Ontario M5S 3H6, Canada

Received August 13, 2007; Revised Manuscript Received October 17, 2007

ABSTRACT

Recently, there has been a great deal of progress in the synthesis of colloidal nanocrystals with tailored physical and chemical properties through control of size and shape, chemical composition, and surface functionalization (Alivisatos, A. P. *Science* 1996, *271* (5251), 933–937; Burda, C.; Chen, X. B.; Narayanan, R.; El-Sayed, M. A. *Chem. Rev.* 2005, *105* (4), 1025–1102). Nanocrystals are thus ideal building blocks for hierarchical self-assembly of topologically complex, multifunctional architectures with properties tuneable at each level of the hierarchy. Here, we present a method, which combines template-assisted self-assembly of nanocrystals with plasma polymerization (Cademartiri, L.; von Freymann, G.; Arsenault, A. C.; Bertolotti, J.; Wiersma, D. S.; Kitaev, V.; Ozin, G. A. *Small* 2005, *1* (12), 1184–1187) to realize hierarchical architectures that both retain the properties of the nanocrystals and offer multifunctionality. As examples, we describe $CoFe_2O_4$–PbS mixed nanocrystal nanorods, which photoluminesce, and align and move in unison with an applied magnetic field and PbS nanocrystal inverse opals, which emit and Bragg diffract near-infrared light. Such hierarchical nanocrystal architectures can be envisioned to spawn new nanotechnologies that integrate multiple functionalities into a single construct.

Self-assembly of nanocrystals within templates is a very relevant topic, and its relevance grows whenever new properties or functions are discovered in nanocrystal assemblies and superlattices.[2,3] Such assemblies are obtained as thin films and are limited to a planar geometry although free-standing nanocrystal membranes have been recently reported.[4] The extension of such assemblies to arbitrary geometries requires the development of programmed interparticle interactions[5,6] or the development of a robust template-assisted self-assembly strategy. In this work, we address this problem by demonstrating with one-dimensional (1D) and three-dimensional (3D) templates how evaporation-induced self-assembly and nanocrystal plasma polymerization allow one to overcome the limitations of all previous methods and obtain free-standing, mechanically stable, multifunctional architectures entirely composed of nanocrystals of choice.

Our methodology is very simple: the template (Figure 1a,e) is immersed in the nanocrystal dispersion (Figure 1b,f); the drying of the solvent leads to a complete infiltration of the template (Figure 1c,g); the nanocrystals are then consolidated within the template by using nanocrystal plasma polymerization and then the template is dissolved (Figure 1d). In the case of polymeric templates, the plasma processing consolidates the nanocrystals and removes the template at the same time (Figure 1h).

* To whom correspondence should be addressed. E-mail: gozin@chem.utoronto.ca.

10.1021/nl072026v CCC: $37.00
Published on Web 11/02/2007

The infiltration of the template is accomplished differently depending on the geometry of the template. The alumina membrane possesses 1D pores of about 200 nm running across its thickness. The membrane is glued at the end of a glass tube, which is capped with a septum and then filled with nanocrystal dispersion. The septum seal is used to avoid evaporation from within the tube. In this setup (Figure 1b), the evaporation proceeds only from the bottom side of the membrane. The dispersion initially flows through forming a droplet at the bottom of the membrane. Such drop evaporates quickly leaving at the bottom of the membrane a gas-permeable nanocrystal film, which prevents nanocrystals from flowing through but still allows evaporation of the solvent. This evaporation-induced flux of solvent drives the nanocrystals to the bottom of the channels forcing them to pack as efficiently as possible. Given the absence of strong interactions between nanocrystals and between the nanocrystals and the channel walls, any energy minima in which each nanocrystal might sit are very shallow and thus allow for a more comprehensive exploration of the energy landscape during the assembly. This, together with the strong driving force of the evaporation-induced flux, constitutes one of the ideal conditions to obtain ordered assembly.

The infiltration of 3D interconnected templates was performed following the same principles outlined above but with a key difference. A cover slip was placed on top of the opal sample and a small amount of nanocrystal dispersion

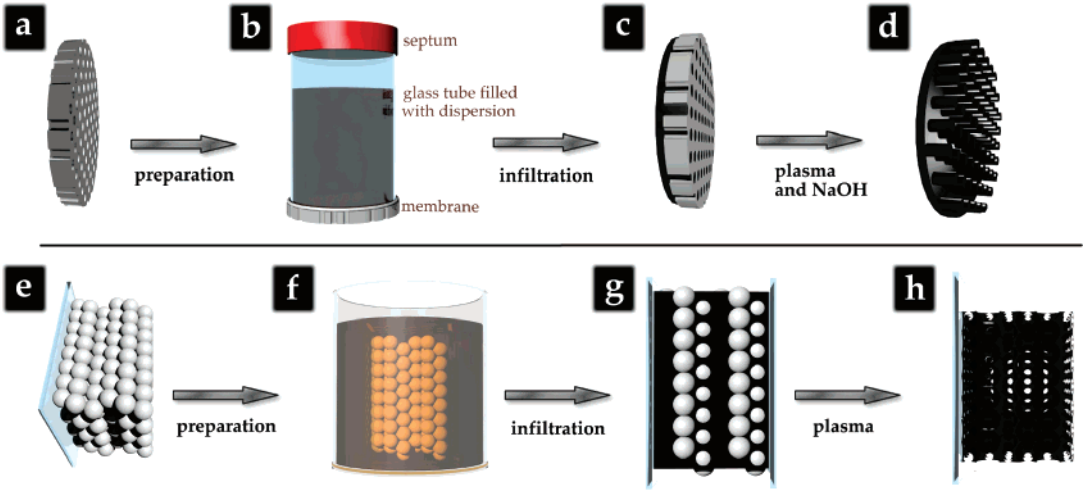

Figure 1. Template-assisted nanocrystal self-assembly: (a−d) these panels show infiltration of an alumina template with colloidal nanocrystals. The template (a) is attached to a glass tube shown in (b). The tube is sealed using a rubber septum to restrict solvent evaporation to that which takes place through the template nanochannels, and then the colloidal nanocrystal dispersion is injected into the tube. As the solvent evaporates, the nanocrystals are pulled into and pack inside the template channels yielding the infiltrated template shown in (c). Air plasma nanocrystal polymerization and selective removal of the template yield free-standing nanocrystal nanorods (d). (e−h) These panels show infiltration of an opal with colloidal nanocrystals. First, the opal is deposited onto a substrate (e) and subsequently submerged in a dispersion of colloidal nanocrystals (f). As the solvent evaporates, the nanocrystals pack inside the voids within the opal as shown in (g). Selective removal of the opal template yields a freestanding nanocrystal inverse opal (h).

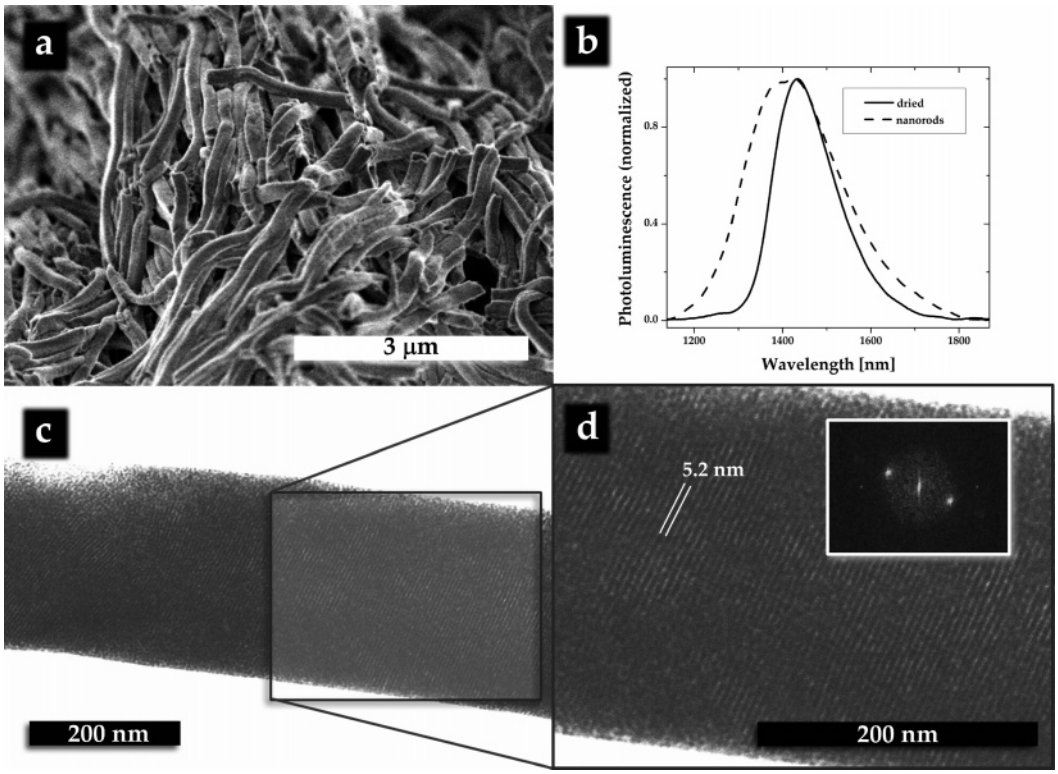

Figure 2. PbS nanocrystal nanorods: (a) Low-magnification SEM image showing long, flexible PbS nanocrystal nanorods. (b) This panel shows PL spectra of colloidal PbS nanocrystals and the dry nanocrystal nanorods demonstrating that the nanocrystals comprising the rods retain their PL and therefore their excitonic confinement. (c) High-magnification TEM image of a PbS nanocrystal nanorod and (d) a magnified portion of the same image. The magnified region clearly shows that infiltrated nanocrystals form an ordered superlattice. The inset shows the FFT image that further highlights the long-range order.

was allowed to diffuse into the gap between the opal substrate and the cover slip effectively squeezing the opal between the substrate and the cover slip. This sandwiched structure was then completely immersed into a highly concentrated (20−50 mg/mL) nanocrystal dispersion that was allowed to evaporate. This method ensured a complete infiltration of the opal and avoided the formation of an overlayer.

To obtain nanocrystal nanorods, we used the commercially available Whatman Anopore Anodisc 13 membranes. These are circular discs of alumina with a diameter of 13 mm,

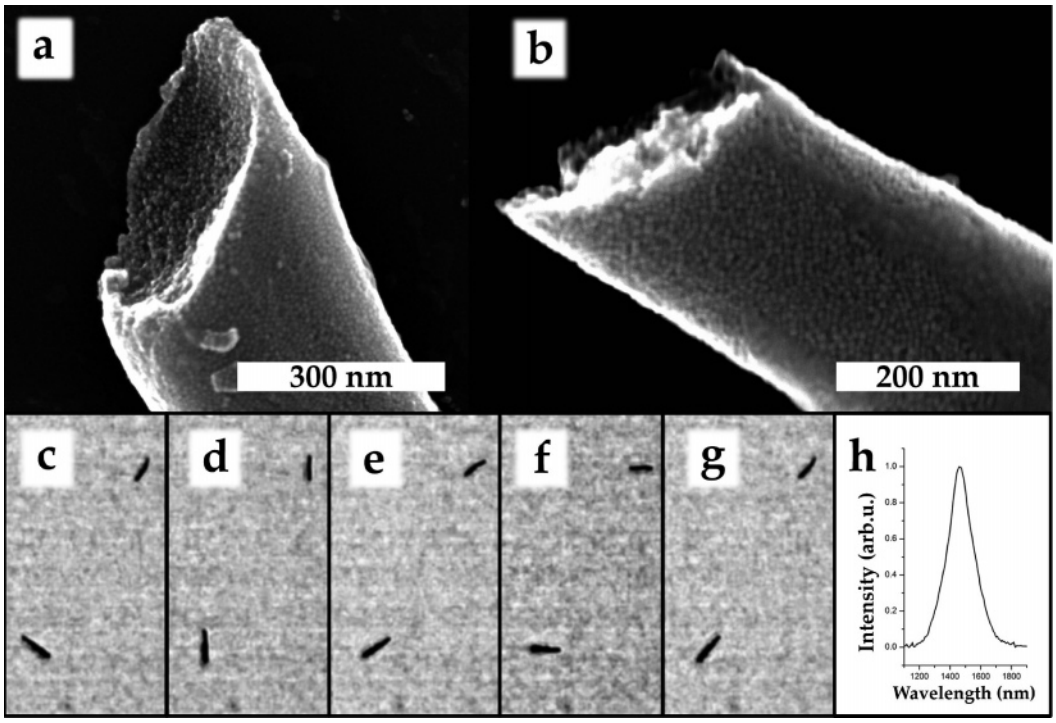

Figure 3. Magnetic and multifunctional nanocrystal nanorods: panel (a) shows an SEM image of a $CoFe_2O_4$ nanocrystal nanorod; (b) is an SEM image of a $CoFe_2O_4$−PbS mixed nanocrystal nanorod. (c−g) These panels are frames from a movie taken in an optical microscope that shows $CoFe_2O_4$−PbS mixed nanocrystal nanorods suspended in a drop of water that move synchronously in response to an external magnetic field. In (c) the nanocrystal nanorods have not yet been subjected to the field and are not parallel. Once the field is applied in (d), the nanocrystal nanorods line up with the field. As the direction of the field is rotated first clockwise by about 90° and then counter clockwise, panels (e−g) show the nanocrystal nanorods always remaining aligned and rotating with the external magnetic field; (h) PL spectrum of the mixed nanocrystal nanorods still within the template.

thickness of 60 μm, and ~200 nm average channel diameter. These membranes were infiltrated with colloidal PbS and $CoFe_2O_4$ nanocrystals in hexane. The lead sulfide nanocrystals were monodisperse enough to show a photoluminescence (PL) peak with full-width at half-maximum (FWHM) of about 60−80 meV. The size of the nanocrystals could be varied between 4.1 to 6.4 nm corresponding to a photoluminescence peak ranging from 1180 to 1580 nm. The polydispersity was evaluated by high resolution transmission electron microscopy (HRTEM) and was found to be around 6% without any size selective precipitation. The $CoFe_2O_4$ nanocrystals were shown to be superparamagnetic and had a size of approximately 10 nm and a polydispersity of 10−15% depending on the sample.[7]

Once the nanocrystals are infiltrated and densely packed they must be consolidated to obtain free-standing structures upon the removal of the template. Room-temperature coalescence,[8] sintering,[9] "shrink wrapping" in polymers,[10] and a thin layer of titania/polymer composite[11] have all been reported. Coalescence and sintering produce nano- or polycrystalline products where excitonic confinement in individual nanocrystals is often compromised and so are the majority of the size-dependent properties of the nanocrystal building blocks. The elevated temperatures required for sintering also can lead to grain growth according to ripening mechanisms that increase the average size of the particles and substantially decrease their monodispersity. The shrink wrapping techniques introduce organic sheaths that tend to be chemically unstable and often exhibit poor performance in electronic applications.

Nanocrystal plasma polymerization is a new and alternative method for consolidating nanocrystal superlattices without the addition of organics or the loss in excitonic confinement. Exposing nanocrystal species to low-power air plasma at room temperature can remove all of the organic capping ligands and traps the nanocrystals in an inorganic amorphous matrix, which mechanically stabilizes the nanocrystals while keeping their surfaces well passivated.[1] After infiltration, the alumina membrane was exposed to a 5 W air plasma for 48 h. Following the plasma treatment, the template was dissolved in 1 M $NaOH_{(aq)}$, and the nanocrystal nanorods were washed in doubly distilled water to remove any residual base. Figure 2 shows PbS nanocrystal nanorods that were obtained after removal of the alumina template.

Figure 2a shows a low-magnification scanning electron microscopy (SEM) image of the nanocrystal nanorods, which are flexible and free-standing, consistent with previous results on thin films.[1] Figure 2b is a comparison of the PL spectra of the colloidal PbS nanocrystals in solution and of the PbS nanocrystal nanorods. The rods exhibit PL comparable to that of the nanocrystals indicating that excitonic confinement is preserved. The PL peak of the nanorods is just slightly widened toward the blue. This could be because the plasma treatment oxidizes some of the material from the surface of PbS nanocrystals, thereby creating a population of smaller nanocrystals at the surface of the rods, which would exhibit

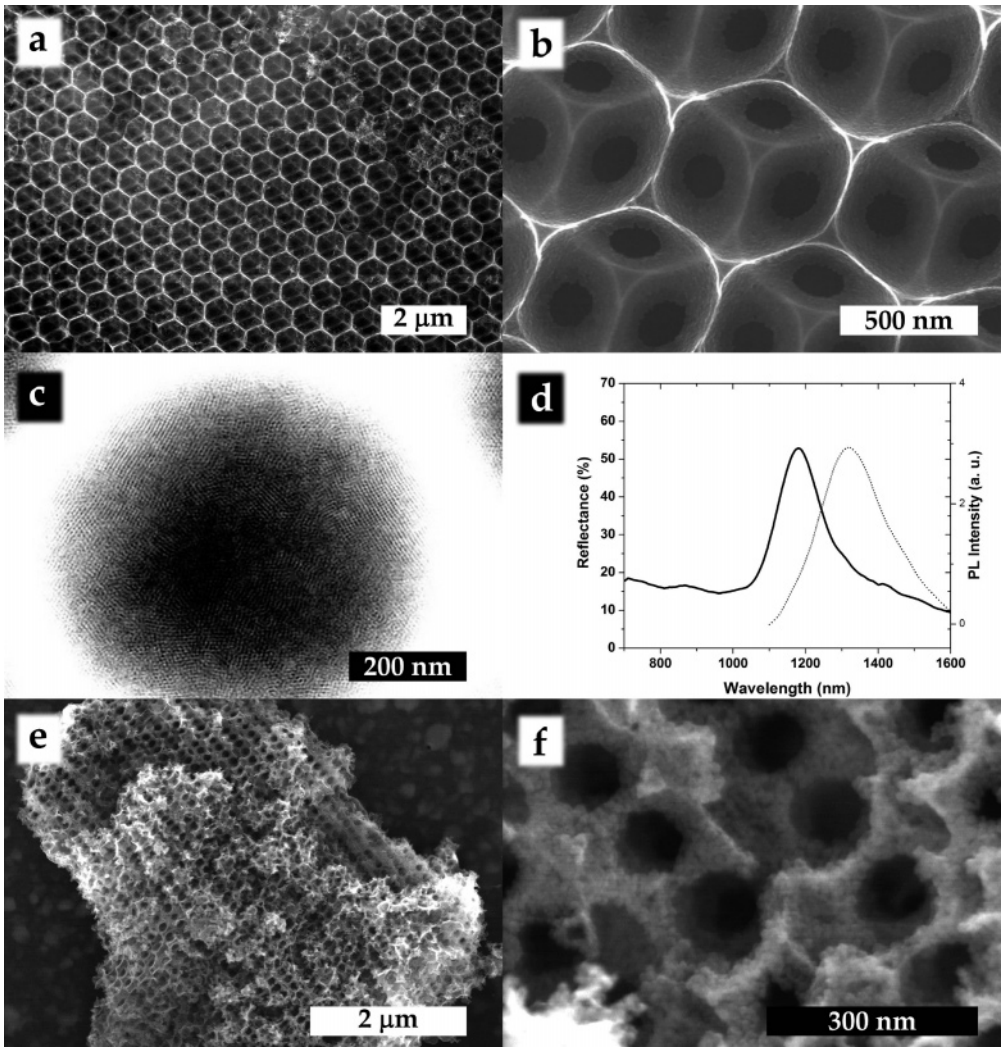

Figure 4. PbS and $CoFe_2O_4$ nanocrystal inverse opals: (a) low-magnification SEM image of a PbS nanocrystal inverse opal and (b) higher magnification of the same opal. (c) Z-contrast TEM image of a PbS nanocrystal inverse opal clearly showing that the nanocrystals have formed ordered domains. (d) The dotted curve is the PL spectrum of the PbS nanocrystal inverse opals, while the solid curve is the reflectance spectrum of the same structure. (e,f) These panels show low- and high-magnification SEM images of $CoFe_2O_4$ nanocrystal inverse opals, respectively.

a blue-shifted PL. It is important to stress that the process presented here has not been optimized for PL emission intensity and FWHM. Our efforts have not yet come close to fully exploring the vast range of possible plasma treatment parameters and their effect on the properties of the plasma polymerized nanocrystal architectures.

Figure 2c is a TEM image of a nanorod extending from the left to the right of the frame; Figure 2d is a magnified region of 2c and clearly shows that the nanorod is comprised of a well-ordered nanocrystal superlattice. To obtain this image, the primary electrons of the TEM had to traverse the full 200 nm thickness of the nanocrystal nanorod, which is only possible along nanocrystal superlattice crystal planes and demonstrates that the superlattice ordering extends throughout the full thickness of the rod. Each of these ordered domains inside the rods extends for hundreds of nanometers. The inset shows the fast Fourier transform (FFT) image, which further highlights the long-range order. Figure 1 in Supporting Information shows ordered domains of nanocrystals on the surface of the PbS nanorods.

Much like the PbS nanocrystal nanorods, the $CoFe_2O_4$ nanocrystals also faithfully replicate the alumina template and form free-standing nanorods, which retain the properties, in this case magnetism, of their nanocrystal building blocks. Figure 3 shows a selection of magnetic and multifunctional nanorods.

Figure 3a shows a high-magnification SEM image of a $CoFe_2O_4$ nanorod. The individual nanocrystal building blocks are clearly visible, and the image demonstrates that the nanocrystal packing is dense and complete throughout the thickness of the rod. Figure 3b is a high-magnification SEM image of a $CoFe_2O_4$−PbS mixed nanocrystal nanorod clearly showing the individual nanocrystal building blocks as well. Figure 3c−g shows two of these mixed nanocrystal nanorods suspended in a drop of water and moving in synchrony in response to an external magnetic field. Before the application of the field in 3c, the rods are randomly oriented with respect to one another. Once the field is applied in 3d, the rods become magnetized and line up with the field; as the field is rotated in the plane of the rods, they follow and remain

parallel to the field, as shown in 3e−g. The full video showing the movement of the mixed nanorods is included in the Supporting Information. Figure 3h shows a normalized PL spectrum of the mixed $CoFe_2O_4$−PbS nanorods before release from the template, confirming that these rods are multifunctional and retain the original properties of both their photoluminescent and magnetic nanocrystal building blocks.

The synthesis method described here is quite general and is not limited to the nanocrystal species or the templates discussed here. CdS,[1] Bi_2S_3,[13] and Fe_3O_4 are examples of other functional, plasma polymerizable nanocrystals that could form nanocrystal nanorods. Furthermore, any template can be used as long as it is in the appropriate size scale and can be selectively removed.

Synthetic opals fabricated through evaporation-induced self-assembly[14] of latex spheres constitute another class of template materials, which also provide photonic crystal functionality, that is, the possibility of controlling the propagation of light by a modification of the photonic density of states through a periodic modulation of the dielectric constant. In more "functional" terms, photonic crystals and opals in particular can Bragg diffract light from the ultraviolet through the visible to the near-infrared spectral range depending on the period of the lattice and the dielectric contrast between the material and air. When an opal is used as a template, the structure that is obtained upon removal of the original template is called an inverse opal. When made from nanocrystals, these inverse structures also exhibit photonic crystal properties and have been the focus of intense investigation because of their potential for possessing a full photonic band gap due to the high refractive index of semiconductor nanocrystals.[15−17]

Our methodology allows for the formation of inverse opals of high quality. Figure 4 shows the nanocrystal inverse opals synthesized using this method.

As Figure 4a,b shows, PbS nanocrystals accurately replicate the geometry of the opal template to form a self-supporting inverse structure. Also in this case, PbS nanocrystals show a pronounced tendency to organize in ordered domains, even under such topologically complex confinement conditions (Figure 4c). The dotted curve in Figure 4d shows the PL spectrum of PbS inverse opal demonstrating that the building block nanocrystals retain their excitonic confinement in the final inverse structure. The solid curve, which represents the Bragg optical reflectance of the inverse opal, confirms that PbS nanocrystals faithfully replicated the geometry of the opal template to form an inverse opal with photonic crystal properties. Figure 4e,f shows similar free-standing inverse opals made from $CoFe_2O_4$ nanocrystals. It is worth noting that the resolution of this infiltration and consolidation methodology is only limited by the size of the nanocrystals.

In summary, we have shown promising results of a new casting technique, which allows for the preparation of virtually arbitrary architectures entirely made of nanocrystals in a way that is compatible with flexible substrates. Such architectures are herein demonstrated to show multiple functions originating from both the nanometer to micron length scales of the nanocrystals and the architectures, respectively. In addition, our results strongly suggest that by controlling the infiltration protocols it is possible to achieve superlattice ordering in nanocrystal nanorod and inverse opal assemblies even under the most complicated confinement conditions.

Acknowledgment. G.A.O. is a Government of Canada Research Chair in Materials Chemistry and Nanochemistry. He is deeply indebted to the Natural Sciences and Engineering Research Council (NSERC) of Canada for financial support for this work. A.G. and L. C thank the University of Toronto for scholarship support of their research. We thank Sebastien Fournier-Bidoz for technical advice on alumina membranes. Author contributions: G.A.O. developed the original concept; A.G. designed and performed the experiment on the membranes; L.C. designed and performed the experiments on the opals; L.C. synthesized the nanocrystals; U.K. fabricated the opal templates; and all authors co-wrote the paper.

Supporting Information Available: Materials and methods; additional SEM of nanocrystal nanorods; video of magnetically actuated nanocrystal nanorods. This material is available free of charge via the Internet at http://pubs.acs.org.

References

(1) Cademartiri, L.; von Freymann, G.; Arsenault, A. C.; Bertolotti, J.; Wiersma, D. S.; Kitaev, V.; Ozin, G. A. *Small* **2005**, *1* (12), 1184−1187
(2) Urban, J. J.; Talapin, D. V.; Shevchenko, E. V.; Kagan, C. R.; Murray, C. B. *Nat. Mater.* **2007**, *6* (2), 115−121.
(3) Shevchenko, E. V.; Talapin, D. V.; Kotov, N. A.; O'Brien, S.; Murray, C. B. *Nature* **2006**, *439*, 55−59.
(4) Lin, Y.; Skaff, H.; Boker, A.; Dinsmore, A. D.; Emrick, T.; Russell, T. P. *J. Am. Chem. Soc.* **2003**, *125* (42), 12690−12691.
(5) DeVries, G. A.; Brunnbauer, M.; Hu, Y.; Jackson, A. M.; Long, B.; Neltner, B. T.; Uzun, O.; Wunsch, B. H.; Stellacci, F. *Science* **2007**, *315* (5810), 358−361.
(6) Kalsin, A. M.; Fialkowski, M.; Paszewski, M.; Smoukov, S. K.; Bishop, K. J. M.; Grzybowski, B. A. *Science* **2006**, *312* (5772), 420−424.
(7) Sun, S. H.; Zeng, H.; Robinson, D. B.; Raoux, S.; Rice, P. M.; Wang, S. X.; Li, G. X. *J. Am. Chem. Soc.* **2004**, *126* (1), 273−279.
(8) Sehayek, T.; Lahav, M.; Popovitz-Biro, R.; Vaskevich, A.; Rubinstein, I. *Chem. Mater.* **2005**, *17* (14), 3743−3748.
(9) Wang, Y.; Lee, J. Y.; Zeng, H. C. *Chem. Mater.* **2005**, *17* (15), 3899−3903.
(10) Marinakos, S. M.; Brousseau, L. C.; Jones, A.; Feldheim, D. L. *Chem. Mater.* **1998**, *10* (5), 1214−1219.
(11) Huang, J. G.; Kunitake, T. *Chem. Comm.* **2005**, (21), 2680−2682.
(12) Norris, D. J.; Vlasov, Y. A. *Adv. Mater.* **2001**, *13* (6), 371−376.
(13) Malakooti, R.; Cademartiri, L.; Akcakir, Y.; Petrov, S.; Migliori, A.; Ozin, G. A. *Adv. Mater.* **2006**, *18* (16), 2189−2194.
(14) Jiang, P.; Bertone, J. F.; Hwang, K. S.; Colvin, V. L. *Chem. Mater.* **1999**, *11* (8), 2132−2140.
(15) Vlasov, Y. A.; Yao, N.; Norris, D. J. *Adv. Mater.* **1999**, *11* (2), 165−169.
(16) Yang, L. L.; Yang, Z. H.; Cao, W. X.; Chen, L.; Xu, J.; Zhang, H. Z. *J. Phys. Chem. B* **2005**, *109* (23), 11501−11504.
(17) Paquet, C.; Yoshino, F.; Levina, L.; Gourevich, I.; Sargent, E. H.; Kumacheva, E. *Adv. Funct. Mater.* **2006**, *16* (14), 1892−1896.

NL072026V